J. Fluid Mech. (1994), *vol.* 277, *pp.* 331–345

Characterization of disturbance propagation in weak shock-wave reflections

By AKIHIRO SASOH AND KAZUYOSHI TAKAYAMA

Shock Wave Research Center, Institute of Fluid Science, Tohoku University, 2-1-1 Katahira, Aoba, Sendai 980, Japan

(Received 26 July 1993 and in revised form 11 April 1994)

Reflections of weak shock waves over wedges are investigated mainly by considering disturbance propagation which leads to a flow non-uniformity immediately behind a Mach stem. The flow non-uniformity is estimated by the local curvature of a smoothly curved Mach stem, and is characterized not only by a pressure increase immediately behind the Mach stem on the wedge but also by a propagation speed. In the case of a smoothly curved Mach stem as is observed in a von Neumann Mach reflection, the pressure increase behind the Mach stem is approximately determined by Whitham's ray-shock theory. The propagation speed of the flow non-uniformity is approximated by Whitham's shock–shock relation. If the shock–shock does not catch up with a point where a curvature of the Mach stem vanishes, a von Neumann Mach reflection appears. The boundary on which the above-mentioned condition breaks results in the transition from a von Neumann Mach reflection to a simple Mach reflection. This idea leads to a transition criterion for a von Neumann Mach reflection, which is algebraically expressed by $\chi_1 = \chi_s$ where χ_1 is the trajectory angle of the point on the Mach stem where the local curvature vanishes and is approximately replaced by $\chi_g - \theta_w$ (χ_g is the angle of glancing incidence, and θ_w is the apex angle of the wedge) and χ_s is the trajectory angle of Whitham's shock–shock, measured from the surface of the wedge. For shock Mach numbers of 1.02 to 2.2 and a wedge angle from 0° to 30°, the domains of a von Neumann Mach reflection, simple Mach reflection and regular reflection are determined by experiment, numerical simulation and theory. The present transition criterion agrees well with experiments and numerical simulations.

1. Introduction

When a planar shock wave reflects over wedges, various reflection patterns appear depending on the shock Mach number M_s and the wedge angle θ_w (Ben-Dor 1991). In particular, when a weak shock wave reflects over a wedge of small θ_w, the reflection of the weak shock appears to be something similar to a simple Mach reflection (SMR). However, the classical theory, that is, von Neumann's three-shock theory (von Neumann 1945), does not always have a physically acceptable solution for this shock reflection pattern. Such a discrepancy between experimental observation and the theory was first pointed out by Birkhoff (1950), who first referred to this discrepancy as the 'von Neumann paradox'.† This terminology originated from the fact that some

† Jahn (1957) and Ben-Dor & Takayama (1992) generalized this paradox and subdivided it into two; according to Ben-Dor & Takayama, the 'first' and 'second' ones. The first one corresponds to the contradiction implied by the existence of a regular reflection RR which is not consistent with the two shock theory. The second one corresponds to the contradiction which arises when a shock reflection pattern resembling a SMR in shape does not conform to the three-shock theory. This study is concerned with the investigation of the second von Neumann paradox.

experimental results did not agree with von Neumann's theory. This terminology – for which von Neumann is not responsible – is a misnomer and often causes misunderstanding of the related phenomena. The terminology, nevertheless, has already become well known among gasdynamicists (Colella & Henderson 1990; Ben-Dor 1991). The essential aspects of this enigmatic problem consist of two questions; first, why that shock reflection pattern appears, and second, under what conditions such a reflection pattern appears. The first question is linked to 'Why does a Mach reflection appear?' The best answer to this question must, in short, settle the von Neumann paradox or the weak shock discrepancy. The second question is most important from a scientific and engineering point of view; weak shock waves commonly appear in condensed matter. Reviews of this problem have been presented by Sakurai *et al.* (1989), Reichenbach (1990), Brown (1992) and Ben-Dor & Takayama (1992).

Ben-Dor (1991) categorized the patterns of possible shock reflections either as regular or irregular reflections. The class of irregular reflections was further subdivided into von Neumann reflections (Colella & Henderson 1990; Ben-Dor 1991) and Mach reflections. The von Neumann reflection corresponds to the second von Neumann paradox (see footnote). Another characteristic of the von Neumann reflection observed in experiments is that an incident shock ('I' shock) and a Mach stem ('M' shock) appear to be a single wave with a smoothly turning tangent. For the sake of simplicity, such a shock wave will hereinafter be referred to as an 'IM' shock. If one denotes any shock reflection in which a reflected wave ('R' shock) is detached from a wall by a Mach reflection MR, the above categorization can be slightly changed. In this case, the above-mentioned shock reflection pattern may be named a Mach reflection of the von Neumann paradox type, or simply, a 'von Neumann Mach reflection NMR'. In this paper, an NMR is defined by a Mach reflection in which an IM shock is continuously curved from its foot to the incident shock. The R shock can be a sound wave.

In the case of SMR, if the effect of viscosity is significant, the intersection of the IM shock with the R shock spreads over a region of finite dimensions. In this region, the variations of pressure and flow deflection angle become continuous. This shock reflection pattern does not belong to that predicted by the three-shock theory. Sakurai (1964) adapted the effect of viscosity in order to interpret the curvature distribution of the NMR. Using a perturbation method, he obtained first-order solutions in which a local curvature of the IM shock was a maximum just below the intersection point of the M shock with the I shock. His solution agreed with experimental observation of shock reflection patterns which the three-shock theory was unable to predict.

In the absence of viscosity, as is explained by Sternberg (1959), if the three shocks intersect with one another at a point, the IM shock cannot have a finite curvature at the point of intersection with the R shock. However, this restriction does not hold if the jump of the flow variables across the reflected wave is infinitesimally small, in other words, if the reflected wave at the intersection is not a shock wave but a compression wave. Colella & Henderson (1990) numerically simulated NMRs and clarified the structure of the reflected shock. Their numerical simulation, using a mesh refinement technique, showed that the reflected wave is not a shock wave but in fact appears to consist of smoothly distributed compression waves in the region where it interacts with the IM shock. The intersection of these compression waves with the M shock is not a single point but spreads over some length. They still postulated that the leading edge of the intersection of the compression waves with the M shock was a triple point, and concluded that since the reflected wave does not appear to be a discontinuity, the three-shock theory cannot be applied at the triple point. Their analysis, even without taking into account the effect of viscosity, well explains the relations between the IM shock

and the R shock in an NMR, and clarifies why the three-shock theory cannot be applied to the NMR.

In the three-shock theory, an M shock is assumed to be straight. However, Glass (1987) pointed out as a general remark on Mach reflection that an M shock can indeed have finite curvatures, which causes inaccurate prediction of the pattern of shock reflections by misusing the three-shock theory. If the gradient of flow variables behind the IM shock is finite, the IM shock has a continuously varying curvature along the entire IM shock (discussed in detail in §2). In such weak shock reflections, the effect of the finite curvature of the IM shock becomes significant. The physical significance associated with the local curvature of the M shock still warrants further investigation (Ben-Dor & Takayama 1992).

Olim & Dewey (1992) revised von Neumann's three-shock theory and assumed that the shape of the M shock was an arc of a circle centred on the wedge surface. This assumption, together with another major revision, effectively leads to better agreement with experimental shock reflection patterns than von Neumann's three-shock theory.

Lighthill (1949) obtained analytically the local curvature of the M shock. In his analysis, disturbances are assumed to be small enough to justify a linearized analysis, that is, to treat the reflected shock as a sound wave. His solution becomes asymptotically accurate for an infinitesimally small inclination angle of the wedge. However, the solution becomes inaccurate as the inclination angle of the wedges is increased.

Tanno (1991) and Sasoh, Takayama & Saito (1992) analysed the variation of local curvature along the M shock of NMRs. Experiments and numerical simulations were conducted for shock Mach number of 1.15. The results obtained by Sasoh *et al.* (1992) showed that on the M shock two special points exist; one is a point at which the curvature vanishes and the other is a point at which the curvature is a maximum. The trajectory of the latter point was found to agree well with that of Whitham's shock–shocks. Although the physical meaning of the point of maximum curvature is not yet fully understood, the point at which the curvature vanishes and that of maximum curvature are closely related to flow mechanisms of how the corner disturbance catches up with the I shock. Therefore, the weak shock reflection should be discussed by taking the propagation of disturbances along the M shock into account.

In this paper, in order to generalize the weak shock reflection phenomena, results of further investigation which mainly illustrate the propagation of disturbances along and behind the IM shock are presented. Details of the present experimental and numerical methods have been presented in Sasoh *et al.* (1992). The test gas was air. A brief description of the present techniques is provided for completeness in Appendix A. Very weak planar shock waves were generated using a shock tube in which a reusable thin rubber membrane, instead of rupturing a Mylar diaphragm, was used (Yang, Onodera & Takayama 1994). This shock tube reproduces shock Mach number M_s with scatter of $\pm 0.2\%$. Only by using this highly reproducible shock tube were planar shock waves with consistent M_s ($M_s < 1.1$) experimentally produced (see also Appendix A).

2. Estimation of flow non-uniformity generated by a wedge

Assume a two-dimensional, and self-similar IM shock as shown in figure 1. The IM shock consists of an incident shock (I shock) and a Mach stem (M shock) which intersect tangentially. The M shock is defined by the curved part of the IM shock (Sasoh *et al.* 1992). P_1 denotes the intersection point between the I and M shocks.

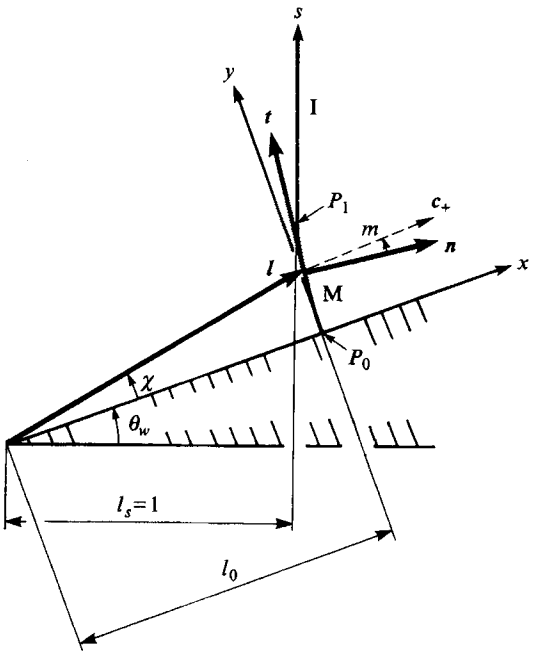

FIGURE 1. Wave shape of a smoothly curved IM shock.

Along the IM shock, take the s-coordinate and its origin P_0 at the foot of the IM shock on the wall. The reflected shock is so weak that flow variables immediately behind the IM shock can be calculated from the Rankine–Hugoniot relations for oblique shock waves.

In the following discussions, all lengthscales are normalized by the horizontal distance between the leading edge of a wedge and an incident shock, that is, $l_s = 1$ in figure 1. Normalized length parameters are denoted by lower cases. $\boldsymbol{l}$ is a pointing vector from the leading edge of the wedge to a point on the IM shock. $\boldsymbol{n}$ and $\boldsymbol{t}$ are unit vectors which are locally normal and tangent to the IM shock, respectively.

The local shock strength is given from the local pressure ratio across the IM shock by

$$\frac{p}{p_0} = 1 + \frac{2\gamma}{\gamma+1}\epsilon, \tag{1}$$

$$\epsilon = M_s^2 |\boldsymbol{l}\cdot\boldsymbol{n}|^2 - 1, \tag{2}$$

where γ is a specific heat ratio, M_s is the shock Mach number of the I shock. The gradient of ϵ in the tangential direction is calculated from (2), such that (see Appendix B),

$$\frac{\mathrm{d}\epsilon}{\mathrm{d}s} = 2M_s^2(\boldsymbol{l}\cdot\boldsymbol{n})(\boldsymbol{l}\cdot\boldsymbol{t})\kappa, \tag{3}$$

where κ is a local curvature of the IM shock. For an IM shock which is concave toward the direction of propagation, as is usually observed in an NMR, κ has a negative value. Equation (3) implies that if the local curvature vanishes, that is, on the straight part of the IM shock, ϵ is constant and the flow behind the IM shock is uniform. A curved shock is associated with a flow non-uniformity behind it.

Figure 2 shows examples of ϵ distributed along the IM shock. Since the IM shock,

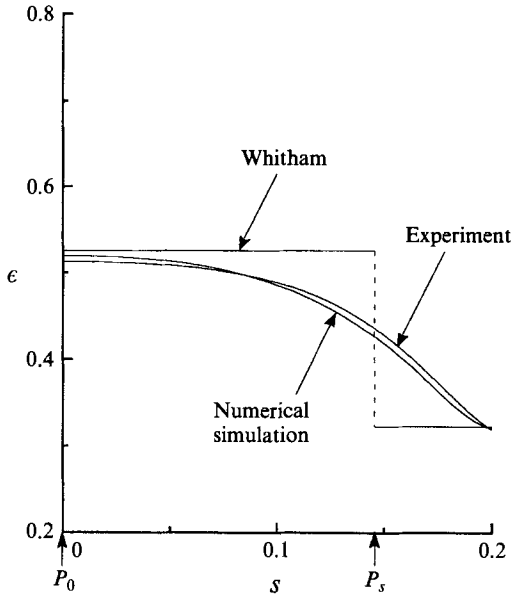

FIGURE 2. Distribution of ϵ along a Mach stem. $M_s = 1.15$, $\theta_w = 15°$.

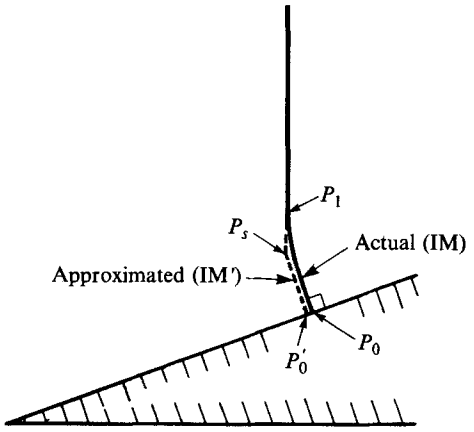

FIGURE 3. Smoothly curved IM shock and its approximated shape, IM′ shock (Whitham's shock–shock).

as observed in the experiment or in the numerical simulation, has a continuously distributed finite curvature, in other words, the IM shock is smoothly curved, the ϵ distribution is also continuous. ϵ is largest on the wedge (at P_0), and is smallest on the I shock.

As shown in figure 3, the actual shape of the IM shock can be approximated by the combination of two planar shock waves. The lower planar shock wave (M′ shock) starts from P_0' and is normal to the wedge surface, the upper one is the extension of the I shock. This configuration of the IM′ shocks appears to be similar to the shape assumed in Whitham's ray–shock theory (Whitham 1957), from which the concept of a shock–shock is derived. The intersection P_s between these two planar shocks is referred to as a shock–shock. With a given combination of M_s and θ_w, the theory determines a unique condition behind the IM′ shocks, that is, a unique combination

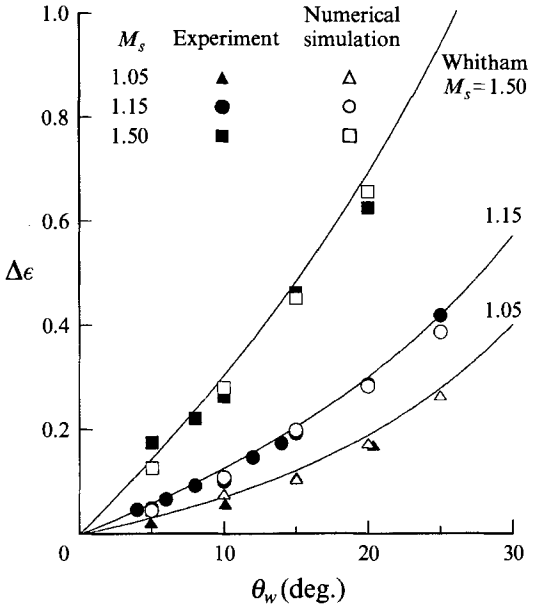

FIGURE 4. $\Delta\epsilon$ *vs.* θ_w.

of χ'_s; the trajectory angle of the shock–shock measured from the wedge surface, l'_0; the distance from the leading edge of the wedge to P'_0 and M'_0; the local shock Mach number on the wedge. l'_0 does not necessarily equal l_0 of the IM shock. The ϵ distribution along IM′ shock is shown also in figure 2. On the straight shock, ϵ is constant. Change in ϵ occurs only at P_s where κ becomes infinity.

Here, let one characterize a flow non-uniformity which is generated by a wedge by

$$\Delta\epsilon \equiv -\int_{\mathrm{IM}} \mathrm{d}\epsilon = M_s^2(l_0^2-1), \tag{4}$$

which is the increase in ϵ on the wedge relative to ϵ on the I shock. As long as one neglects viscosity, the present problem is expressed solely in terms of $(x/t, y/t)$ coordinates (Jones, Martin & Thornhill 1951), implying that, as has been implicitly assumed, the shock shape is self-similar with the elapse of time. Therefore, $\Delta\epsilon$ is determined only from M_s and l_0, and is independent of a curvature distribution between P_0 and P_1. Figure 4 shows the dependence of $\Delta\epsilon$ on θ_w and M_s. $\Delta\epsilon$ which is determined from the experiments is very close to that determined by the numerical simulations. Moreover, the prediction of $\Delta\epsilon$ by the angle of Whitham's shock–shock with the same combination of M_s and θ_w is also close to the above two estimates. In other words, $\Delta\epsilon$ is correctly approximated from Whitham's ray–shock theory even though the actual shock shape does not have such a kink point as the shock–shock does. This tendency is in agreement with the experimental observation by Olim & Dewey (1992).

3. Propagation of flow non-uniformity

In Whitham's ray–shock theory, the trajectory of a shock–shock corresponds to that of a flow non-uniformity propagating along the shock, which is generated by a difference in pressure between two planar shock waves.

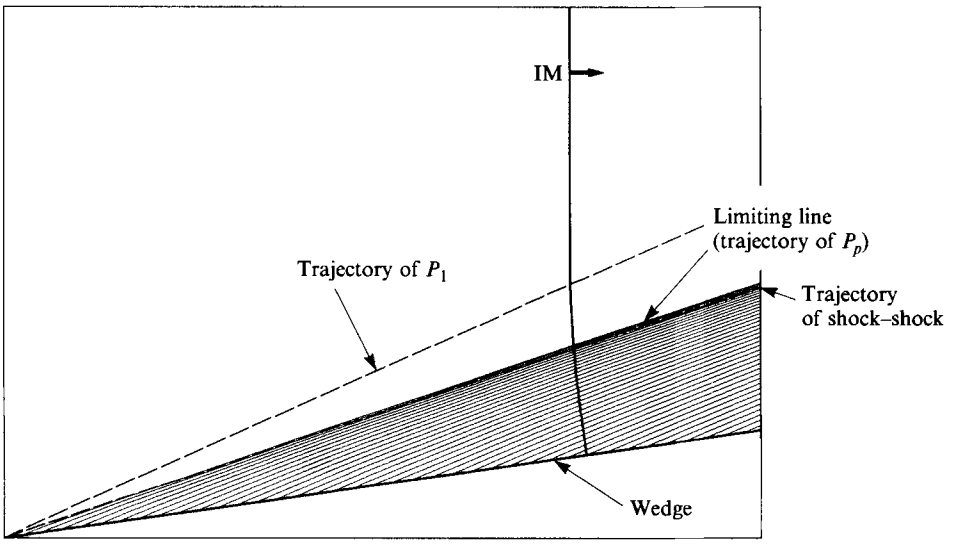

FIGURE 5. Propagation trajectory of disturbances which are generated on a wedge when the IM shock passes. $M_s = 1.15$, $\theta_w = 8°$.

Along a smoothly curved shock wave, the propagation of disturbances can be analysed using the CCW theory (Chester 1954; Chisnell 1957; Whitham 1957), in which the above Whitham's ray–shock theory is included. Applying the CCW theory, the propagation speed of a local disturbance along a smoothly curved shock wave is given by (Whitham 1957)

$$\boldsymbol{c}_{\pm} = |\boldsymbol{l}\cdot\boldsymbol{n}|\,(\boldsymbol{n} \pm \boldsymbol{t}\tan m), \tag{5}$$

$$\tan m = \left[\frac{1-M_n^{-2}}{\lambda(M_n)}\right]^{1/2}, \tag{6}$$

$$\lambda(M_n) = \left(1+\frac{2}{\gamma+1}\frac{1-\mu^2}{\mu}\right)\left(1+2\mu+\frac{1}{M_n^2}\right), \tag{7}$$

$$\mu^2 = \frac{(\gamma-1)M_n^2+2}{2\gamma M_n^2-(\gamma-1)}, \tag{8}$$

$$M_n = M_s(\boldsymbol{l}\cdot\boldsymbol{n}), \tag{9}$$

where m is an angle between $\boldsymbol{c}_+$ and $\boldsymbol{n}$ (see figure 1). Here, $\boldsymbol{c}_+$ represents a wave along the IM shock on which a Riemann invariant is constant (this wave may be referred to as a 'shock characteristic'). It is noted that the propagation speed of $\boldsymbol{c}_+$ is assumed to be determined only by the local shock strength – the effect of non-uniformities in the flow field downstream of the IM shock is not taken into account.

Figure 5 shows propagation trajectories of a disturbance which is generated on the wedge when the IM shock passes. The direction of the propagation is calculated by (6). As seen in this figure, a limiting line exists for the propagation of the disturbances. On the limiting line, $\boldsymbol{c}_+$ is parallel to $\boldsymbol{l}$.

Owing to the self-similarity, flow variables immediately behind the IM shock are constant along lines which pass through the leading edge of the wedge. The speed of propagation of disturbances given by (5) corresponds solely to disturbances generated by a local flow non-uniformity immediately behind the IM shock, that is, by the curvature of the IM shock (see equation (3)). The shock shape or flow variables

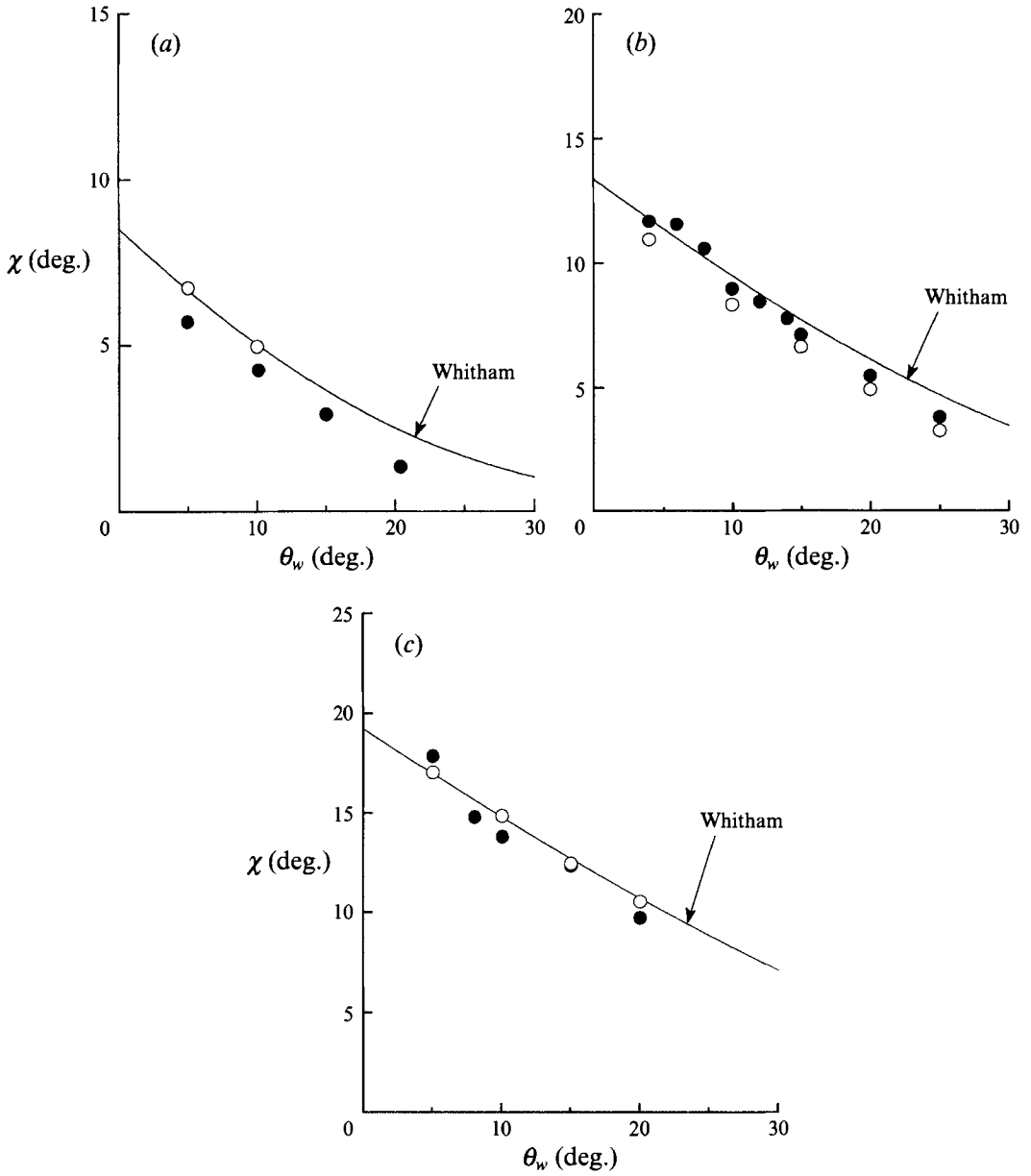

FIGURE 6. Trajectory angles of P_p and of Whitham's shock–shock. (*a*) $M_s = 1.05$, (*b*) $M_s = 1.15$, (*c*) $M_s = 1.50$. ●, experiment; ○, numerical simulation.

immediately behind the IM shock are determined not only by such disturbances but also by those which are continuously generated at points away from the IM shock. The existence of the limiting line implies that only below this limiting line is local shock shape influenced by the disturbances which are generated by the wedge when the IM shock passes. In such a weak shock reflection (as is shown in figure 5), the IM shock is curved even above the limiting line. Here, P_p is defined as a point located on the limiting line. Between P_1 and P_p, the IM shock is influenced by disturbances originating at points far from the IM shock and propagating through the non-uniform flow field behind the IM shock. A disturbance which propagates to P_1 corresponds to that

generated at the leading edge when the IM shock passes (Sasoh 1992, this disturbance will hereinafter be referred to as the first 'leading-edge disturbance').

The condition that $\boldsymbol{c}_+$ becomes parallel to a line which passes through that point and the leading edge is

$$\boldsymbol{l}\cdot\boldsymbol{t} = \boldsymbol{c}_+\cdot\boldsymbol{t} = (\boldsymbol{l}\cdot\boldsymbol{n})\tan m. \tag{10}$$

Above P_p where (10) is satisfied, $\boldsymbol{l}\cdot\boldsymbol{t} > (\boldsymbol{l}\cdot\boldsymbol{n})\tan m$. Below P_p, the inequality sign reverses.

It is found in figure 6 that the trajectory angle of P_p is very close to P_s of Whitham's shock–shock. In Whitham's ray–shock theory, the trajectory of the shock–shock is also a limiting line of the propagation of disturbances generated on the wedge. Therefore, P_p on a smoothly curved IM shock is equivalent to P_s for Whitham's ray–shock theory. It follows that even on a smoothly curved IM shock the propagation of the flow non-uniformity generated by a wedge is characterized by the trajectory of P_p, which is approximately determined by the trajectory of Whitham's shock–shock.

4. Transition criterion

Domains of shock reflection patterns for various combinations of small θ_w and weak shock wave as observed in experiments and numerical simulations are shown in figures 7(*a*) and 7(*b*). Three shock reflection patterns exist as follows:

[A] von Neumann Mach reflection NMR (see figure 8*a*),
[B] Simple Mach reflection SMR,
[C] Regular reflection RR.

Here, a shock reflection pattern in which the length of the M shock is smaller than the resolved shock thickness is classified as a RR; otherwise, it is a Mach reflection. In Mach reflections, a shock reflection pattern in which the minimum radius of curvature is smaller than the resolved shock thickness is classified as a SMR; otherwise it is classified as a NMR. This SMR $\leftrightarrow$ NMR transition criterion will hereinafter be referred to as the 'finite curvature criterion'. Even under conditions close to the transition, a shock shape only gradually changes with M_s or θ_w, thereby causing uncertainty in determining the transition boundaries. Comparing figure 7(*a*) with figure 7(*b*), however, reflection patterns experimentally observed agree with those observed in the numerical simulation within this uncertainty.

In the present study, one can regard a wedge as a disturbance generator. The disturbance behind the IM shock is first generated when the IM shock passes the leading edge of the wedge. The condition for maintaining such a smoothly curved shock shape of the IM shock is that the first-generated leading-edge disturbance intersects with the IM shock (at P_1) above P_p. From P_p to P_1, the shock shape is determined mainly by the leading-edge disturbances. If the leading-edge disturbances are weak enough, they do not generate a steep flow non-uniformity behind the IM shock. In this case, the IM shock still maintains its smoothly curved structure (Colella & Henderson 1990; Ben-Dor & Takayama 1992). This condition is equivalent to the condition that the trajectory angle of P_1 is larger than that of P_p, the latter being approximately determined by the trajectory angle of Whitham's shock–shock, χ_s. Therefore, the SMR $\leftrightarrow$ NMR transition criterion, that is the finite curvature criterion, is expressed by

$$\chi_1 = \chi_s. \tag{11}$$

In (11), χ_1 denotes the trajectory angle of P_1 measured from the wedge surface. If a wedge

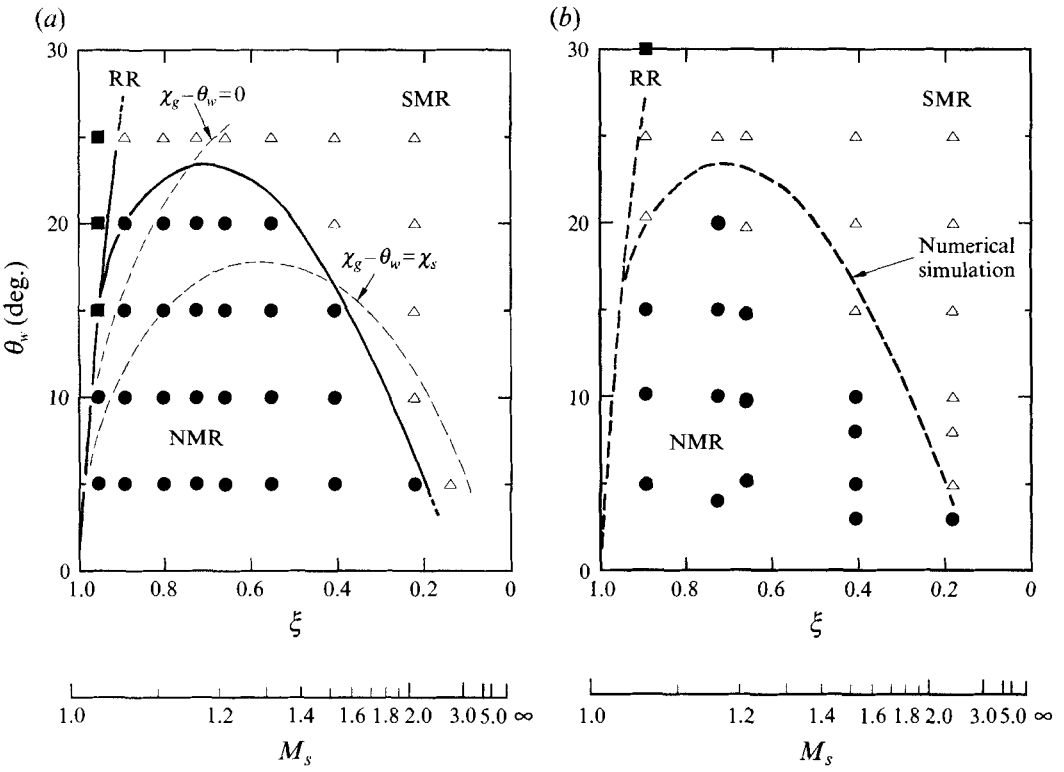

FIGURE 7. Domains of shock reflection patterns observed in the experiment and the numerical simulation. ξ is an inverse pressure ratio across the incident shock. (*a*) Numerical simulation, the left-hand broken line represents the condition of $\chi_g-\theta_w=0$, the right-hand one the condition of $\chi_g-\theta_w=\chi_s$. The solid lines are observed boundaries among different reflection patterns. (*b*) Experiment, the broken lines are the boundaries observed in the numerical simulation shown in (*a*). ●, NMR; △, SMR; ■, RR.

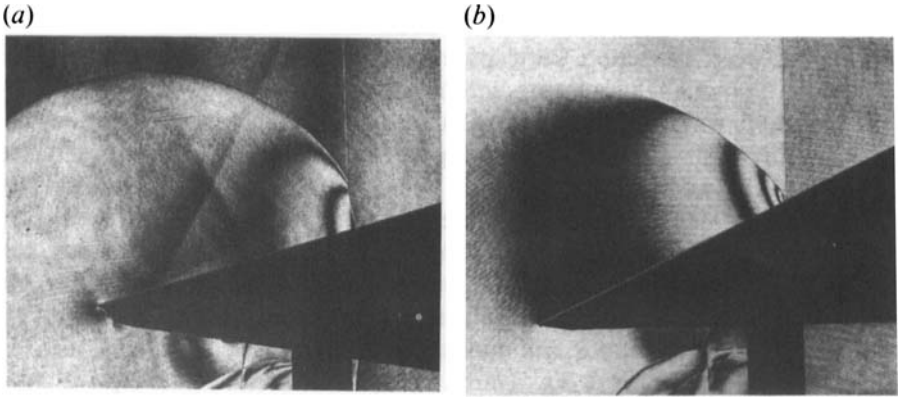

FIGURE 8. Reconstructed interferogram. (*a*) $M_s=1.15$, $\theta_w=15°$ (NMR), (*b*) $M_s=1.05$, $\theta_w=25°$ (close to SMR ↔ NMR and SMR ↔ RR transition boundaries).

angle is small enough to neglect the effect of compression caused by the wedge, the leading-edge disturbances propagate with nearly the speed of sound. In this case, χ_1 is calculated by (Ames 1953)

$$\tan\chi_1 = \tan\chi_g \equiv \left[\frac{(M_s^2-1)\{2+(\gamma-1)M_s^2\}}{(\gamma+1)M_s^4}\right]^{1/2}. \tag{12}$$

For small θ_w, χ_1 is approximately given by $\chi_g-\theta_w$. The stronger the leading-edge disturbance is, the less accurate this approximation becomes.

As is seen in figure 7(*a*), for small θ_w, $\chi_g-\theta_w = \chi_s$ agrees well with the SMR $\leftrightarrow$ NMR transition boundary observed in the experiment and numerical simulation. However, this estimation of the transition boundary becomes progressively less accurate for larger θ_w because here χ_1 is approximated by $\chi_g-\theta_w$.

In the same way, the SMR $\leftrightarrow$ RR transition criterion is expressed by

$$\chi_1 = 0. \tag{13}$$

In Region [C], χ_g is smaller than θ_w; to the zeroth approximation, even leading-edge disturbances cannot catch up with the I shock above the wedge. χ_1 monotonically decreases with increasing θ_w. With increasing θ_w and keeping M_s constant, the NMR $\leftrightarrow$ SMR transition occurs always before the SMR $\leftrightarrow$ RR transition does, because χ_s has a positive value except for $\chi_s = 0$ at $M_s = 1$. However, for very weak incident shock waves ($M_s \leqslant 1.05$), the domain of SMR is very narrow. A shock reflection close to the transition boundaries is shown in figure 8(*b*).

As mentioned in §2, an NMR has two major characteristics; first, the three-shock theory does not have a physically acceptable solution; and secondly, it has finite curvature distribution throughout an IM shock. The above mentioned SMR $\leftrightarrow$ NMR transition criterion, equation (11), is based on the second characteristic.

Colella & Henderson (1990) proposed another type of transition criterion for an NMR. In their experiment, shock reflection pattern begins to deviate from that predicted by von Neumann's three-shock theory under the condition of $\beta_1 = \frac{1}{2}\pi$ (β_1; angle between a reflected shock and a slip line, Henderson 1987; Colella & Henderson 1990). This transition criterion will hereinafter be referred to as the '$\beta_1 = \frac{1}{2}\pi$ criterion'. The $\beta_1 = \frac{1}{2}\pi$ criterion places an experimentally observed limit of applying the three-shock theory, thereby corresponding to the first characteristic of an NMR. Although the $\beta_1 = \frac{1}{2}\pi$ criterion corresponds to a condition for the SMR $\leftrightarrow$ NMR transition, the quantitative accuracy of this criterion has not yet been fully determined. In the three-shock theory, the M shock is assumed to be straight – the curvature equals zero except at a triple point. If the effect of curvature variation along the M shock is taken into consideration, the $\beta_1 = \frac{1}{2}\pi$ condition can be changed, giving a different transition boundary.

In figure 9, some transition boundaries are shown. One corresponds to the finite curvature criterion which is obtained by the present experiments and numerical simulations. Another corresponds to the condition of $\chi_g-\theta_w = \chi_s$, which is an approximate algebraic expression of the finite curvature criterion. The others correspond to the $\beta_1 = \frac{1}{2}\pi$ criterion and to the detachment criterion, the latter of which corresponds to the limit of physically acceptable solution to the two-shock theory (Henderson 1987).

Within the uncertainties associated with the above-mentioned data processing and the algebraic approximation, $\chi_g-\theta_w = \chi_s$ agrees with the finite-curvature criterion. However, these two estimates do not coincide with the $\beta_1 = \frac{1}{2}\pi$ criterion.

Olim & Dewey (1992) suggested from their experimental observation that in a (θ_w,

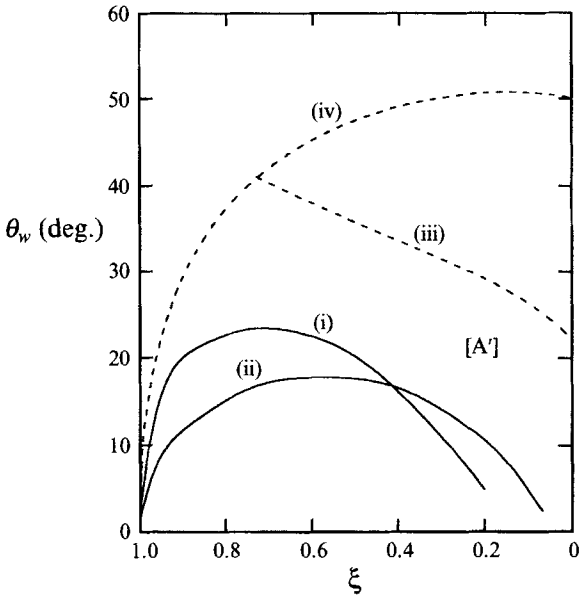

FIGURE 9. Three NMR↔SMR transition boundaries; (i) finite curvature criterion observed in the experiments and the numerical simulations (figure 7*a*, *b*), (ii) $\chi_\varphi - \theta_w = \chi_s$ and (iii) $\beta_1 = \frac{1}{2}\pi$ criterion, and a RR↔SMR transition boundary; (iv) detachment criterion.

M_s)-plane, there exists a region in which an IM shock has a kink at the intersection with the R shock though the three-shock theory does not have any physically acceptable solutions (they named such a shock reflection pattern a 'weak Mach reflection'. In this paper, this shock wave reflection pattern is categorized into an SMR because it has a kink). Region [A'] in figure 9 between the curves corresponding to the $\beta_1 = \frac{1}{2}\pi$ criterion and to the finite-curvature criterion may represent the pattern of this shock reflection. The existence of Region [A'] may lead to a compromise with the difference between the finite-curvature criterion and the $\beta_1 = \frac{1}{2}\pi$ criterion.

Both of the finite-curvature criterion and the $\beta_1 = \frac{1}{2}\pi$ criterion discriminate between a different weak shock reflection pattern with an SMR. In order for that weak shock reflection pattern to appear, the shock wave need not necessarily be weak. As is seen in figures 7(*a*) and 7(*b*), an NMR appeared even for $\xi < 0.2$ (or $M_s > 2$). This may imply that the condition for an NMR is based not on the strength of a shock wave itself but on the strength of the disturbances generated by the wedge surface. In this way, these two criteria describes the same physics but using different formulations. The quantitative relation between these two criteria warrants further investigation.

5. Conclusion

A flow non-uniformity generated by a wedge can be characterized by $\Delta\epsilon$. Even for a smoothly curved shock front shape, $\Delta\epsilon$ is approximately determined from Whitham's ray–shock theory. The propagation trajectory of this flow non-uniformity is represented by the trajectory of P_p which is the limiting line of the propagation of disturbances generated at the wedge when an IM shock passes. The trajectory of P_p is approximately determined by that of Whitham's shock–shock, which is analytically determined solely by giving M_s and θ_w. As long as P_p does not catch up with P_1, the IM shock maintains its smoothly curved structure, thereby forming an NMR. When

the disturbance generated by a wedge becomes strong enough for P_p to catch up with P_1, an NMR terminates and an SMR appears.

From the above-mentioned idea, a new transition criterion for an NMR, the finite-curvature criterion, has been developed. This criterion discriminates between a shock reflection pattern in which an IM shock does not have a kink and a SMR. The criterion is algebraically expressed by $\chi_1 = \chi_s$ or approximately $\chi_g - \theta_w = \chi_s$. The condition that the three-shock theory does not have a physically acceptable solution leads to another transition criterion such as the $\beta_1 = \frac{1}{2}\pi$ criterion. These two transition criteria do not coincide with each other. Quantitative relation between these two criteria warrants further investigation.

At any event, the (second) von Neumann paradox is caused by limitations in the application of the three-shock theory to shock reflection patterns in which the flow field around such a distinct point as a triple point in an SMR is not sufficient to determine the entire reflection characteristics. In order to fully understand such weak shock wave reflections, clarification of the role played by disturbance propagation is essential.

The authors would like to thank Professors John H. Lee and Joseph Falcovitz, visiting professors of Institute of Fluid Science, Tohoku University, Japan, for their discussions and to Professor A. Sakurai, Tokyo Denki University and Professor F. Higashino, Tokyo Noko University, for their suggestions. The authors would like to thank Dr T. Saito, Cray Research Japan Inc. for his conducting numerical simulation for this project and Messrs O. Onodera, J. Yang, H. Ojima and T. Ogawa, the Shock Wave Research Center of Tohoku University, for conducting the experiment. This study was supported in part by a Grant-in-Aid for Scientific Research for Priority Area Shock Waves no. 03238101 offered by the Ministry of Education, Science and Culture of Japan.

Appendix A. Methods of experiment and numerical simulation

Experiments are conducted using a 60 mm × 150 mm cross-sectional shock tube equipped with a holographic interferogram. In order to test for a wide range of M_s, two driver sections were used; one for $M_s = 1.05 \sim 1.20$, another for $M_s \geqslant 1.15$. A flexible, thin rubber membrane which moves quickly and consistently was used in place of a conventional Mylar diaphragm (Yang *et al.* 1994). This driver system enabled very weak planar shock waves to be generated. Scatter of M_s was considerably improved – within 0.2%. However, this apparatus limits, owing to the strength of the membrane, the M_s only to a weak shock region. Another driver section utilizes Mylar diaphragm. The thickness of a diaphragm determines its rupture pressure. This conventional type driver section was used to generate relatively strong plane shocks $M_s \geqslant 1.15$. The error in M_s by this driver section was 3%.

A flow-visualization experiment was carried out using double exposure holographic interferometry (Takayama 1983). In this study, only weak shock waves were treated. Therefore, fringes in a reconstructed hologram correspond to isopycnics. Sensitivity of one fringe shift is approximately 4% of the density under the standard condition. A shock shape was identified from an unreconstructed hologram, which is equivalent to a shadowgraph, using the combination of a CCD camera and an image processor (SPICA-2, Japan Avionics). The image of the hologram is converged into 480 × 400 pixel data.

Numerical simulation was conducted using Harten and Yee's TVD finite difference scheme (Harten 1983; Yee 1987) applied to the two-dimensional unsteady Euler

equations. 800×250 grid points covered a computational domain. Downstream boundary conditions were determined by normal shock relations associated with a given M_s. Computation was conducted until flow at boundaries, except on the wedge, became disturbed by reflected waves. In the numerical simulation, the shock shape was identified by an isopycnic of an appropriate value. A Cray YMP 8/8128 of the Supercomputer Center, Institute of Fluid Science, Tohoku University was used.

Both in the experiment and in the numerical simulation, a shock shape which was given by discrete data was processed by a smoothing technique in which a *B*-spline function was used. The shape of the IM shock of present interest does not have a kink point but has a continuous curvature distribution. Under this restriction, the selection of the order and the number of the nodes was carefully made. If the order of the spline function is too high, the calculated curvature contains high wavenumber components which are physically meaningless. As long as the second derivative of a shock shape was continuous but not constant, the order of the spline function was selected to be as low as possible; a third order with two nodes, or a fourth order when the number of the nodes exceeded two. The number of the nodes, two to four in this study, was selected so as to obtain the best fit to the discrete data. Because of a finite spatial resolution, the calculated value of the curvature is finite. In cases where the radius of curvature was found to be smaller than the spatial resolution, the curvature was set to be infinite. The spatial resolution is determined by the observed thickness of an IM shock. In the experiment, the thickness depends on the quality of the shadowgraph. In the numerical simulation, it depends both on numerical viscosity and on grid spacing.

Appendix B. Derivation of equation (3)

On the (x, y)-coordinates in figure 1 (the origin is P_0), the components of $\boldsymbol{l}$, $\boldsymbol{n}$ and $\boldsymbol{t}$ are as follows:

$$\boldsymbol{l} = \begin{pmatrix} l_0 + x \\ y \end{pmatrix}, \tag{A 1}$$

$$\boldsymbol{n} = \frac{1}{[1 + (\mathrm{d}x/\mathrm{d}y)^2]^{1/2}} \begin{pmatrix} 1 \\ -\dfrac{\mathrm{d}x}{\mathrm{d}y} \end{pmatrix}, \tag{A 2}$$

$$\boldsymbol{t} = \frac{1}{[1 + (\mathrm{d}x/\mathrm{d}y)^2]^{1/2}} \begin{pmatrix} \dfrac{\mathrm{d}x}{\mathrm{d}y} \\ 1 \end{pmatrix}. \tag{A 3}$$

Here, the shape of the IM shock is expressed by $x = x(y)$. Using the relations;

$$\frac{\mathrm{d}}{\mathrm{d}s} = \frac{1}{[1 + (\mathrm{d}x/\mathrm{d}y)^2]^{1/2}} \frac{\mathrm{d}}{\mathrm{d}y}, \tag{A 4}$$

$$\kappa = \frac{-\mathrm{d}^2x/\mathrm{d}y^2}{[1 + (\mathrm{d}x/\mathrm{d}y)^2]^{3/2}}, \tag{A 5}$$

the following simple relations are derived:

$$\frac{\mathrm{d}\boldsymbol{l}}{\mathrm{d}s} = \boldsymbol{t}, \tag{A 6}$$

$$\frac{\mathrm{d}\boldsymbol{n}}{\mathrm{d}s} = \kappa \boldsymbol{t}. \tag{A 7}$$

From (2), (A 6) and (A 7), using the relation $t\cdot n = 0$,

$$\begin{aligned}\frac{\mathrm{d}\epsilon}{\mathrm{d}s} &= 2M_s^2(l\cdot n)\left(\frac{\mathrm{d}l}{\mathrm{d}s}\cdot n + l\cdot\frac{\mathrm{d}n}{\mathrm{d}s}\right)\\ &= 2M_s^2(l\cdot n)\,[t\cdot n + l\cdot(\kappa t)]\\ &= 2M_s^2(l\cdot n)\,(l\cdot t)\,\kappa. \end{aligned} \tag{A 8}$$

REFERENCES

AMES 1953 Equations, tables and charts for compressible flow. Ames Aeronautical Laboratory Rep. 1135.

BEN-DOR, G. 1991 *Shock Wave Reflection Phenomena*. Springer.

BEN-DOR, G. & TAKAYAMA, K. 1992 The phenomena of shock reflection – a review of unsolved problems and future research needs. *Shock Waves Intl J.* **2**, 211–223.

BIRKHOFF, G. 1950 *Hydrodynamics, a Study in Logic, Fact and Similitude*. Princeton University Press, NJ.

BROWN, L. (ED.) 1992 *Book of Abstracts, the 10th Mach Reflection Symposium, Denver.*

CHESTER, W. 1954 The quasi cylindrical shock tube. *Phil. Mag.* **45**, 1293–1301.

CHISNELL, R. F. 1957 The motion of a shock wave in a channel with applications to cylindrical and spherical shock waves. *J. Fluid Mech.* **2**, 286–298.

COLELLA, P. & HENDERSON, L. F. 1990 The von Neumann paradox for the diffraction of weak shock waves. *J. Fluid Mech.* **213**, 71–94.

GLASS, I. I. 1987 Some aspects of shock-wave research. *AIAA J.* **25**, 214–229.

HARTEN, A. 1983 High resolution schemes for hyperbolic conservation laws. *J. Comput. Phys.* **49**, 357–393.

HENDERSON, L. F. 1987 *Z. angew. Math. Mech.* **67**, 73–86.

JAHN, R. G. 1957 Transition processes in shock wave interactions. *J. Fluid Mech.* **2**, 33–52.

JONES, D. M., MARTIN, P. M. E. & THORNHILL, C. K. 1951 A note on the pseudo-stationary flow behind a strong shock diffracted or reflected at a corner. *Proc. R. Soc. Lond.* A **209**, 238–248.

LIGHTHILL, M. J. 1949 They diffraction of blast. I. *Proc. R. Soc. Lond.* A **198**, 454–470.

NEUMANN, J. VON 1945 Refraction, intersection and reflection of shock waves. *NAVORD Rep.* 203–45, Navy Dept, Bureau of Ordinance, Washington, DC.

OLIM, M. & DEWEY, J. M. 1992 A revised three-shock solution for the Mach reflection of weak shocks ($1.1 < M_i < 1.5$). *Shock Waves Intl J.* **2**, 167–176.

REICHENBACH, H. (ED.) 1990 *Book of Abstracts, the 9th Mach Reflection Symposium, Freiburg.*

SAKURAI, A. 1964 On the problem of weak Mach reflection. *J. Phys. Soc. Japan* **19**, 1440–1450.

SAKURAI, A., HENDERSON, L. F., TAKAYAMA, K., WALENTA, Z. & COLELLA, P. 1989 On the von Neumann paradox of weak Mach reflection. *Fluid Dyn. Res.* **4**, 333–345.

SASOH, A., TAKAYAMA, K. & SAITO, T. 1992 A weak shock wave reflection over wedges. *Shock Waves Intl J.* **2**, 277–281.

STERNBERG, J. 1959 Triple-shock-wave intersections. *J. Fluid Mech.* **2**, 179–206.

TAKAYAMA, K. 1983 Application of holographic interferometry to shock wave research. *Proc. SPIE* **398**, 174–181.

TANNO, H. 1991 Study on weak shock wave reflections. Master dissertation, Tohoku University (in Japanese).

WHITHAM, G. B. 1957 A new approach to problems of shock dynamics. Part 1. Two-dimensional problems. *J. Fluid Mech.* **2**, 145–171.

YANG, J., ONODERA, O. & TAKAYAMA, K. 1994 Design and performance of a quick opening shock tube using a rubber membrane for weak shock wave generation. *JSME J.* (in Japanese) **60**, 473–478.

YEE, H. C. 1987 Upwind and symmetric shock-capturing schemes. *NASA Tech. Mem.* 89464.